International Journal of GEOMATE, June., 2021, Vol.20, Issue 82, pp.93-100
ISSN: 2186-2982 (P), 2186-2990 (O), Japan, DOI: https://doi.org/10.21660/2021.82.j2089
Geotechnique, Construction Materials and Environment

GAS TRANSPORT PARAMETERS OF RECYCLED CONCRETE AND CLAY BRICK AGGREGATE BLENDED WITH AUTOCLAVED AERATED CONCRETE GRAINS

Van Nam PHAM[1], *Akira KATO[1], Hoang Giang NGUYEN[2], Van Tuan NGUYEN[2], Quang Minh PHAN[2], and Ken KAWAMOTO[1,2]

[1]Graduate School of Science and Engineering, Saitama University, Japan; [2]National University of Civil Engineering, Vietnam

*Corresponding Author, Received: 16 Jan. 2021, Revised: 04 Feb. 2021, Accepted: 07 Mar. 2021

ABSTRACT: Gas diffusivity (D_p/D_0: the ratio of gas diffusion coefficient, D_p, to gas diffusion in free air, D_0) and air permeability (k_a), and their variations with air-filled porosity (ε) play key roles in surface gas exchange and vapor transport in permeable pavement and water-retentive pavement systems. This study carried out a series of laboratory measurements of D_p/D_0 and k_a for graded recycled concrete (RC) and clay brick (RCB) aggregates, and RC and RCB blended with autoclaved aerated concrete (AAC) grains at proportions of 20% and 40%. The tested samples were saturated after compaction, and the D_p/D_0 and k_a were measured during the drying process from saturation to air-dry. Results showed that D_p/D_0 and k_a of graded RC and RCB decreased most with increased proportions of AAC grains; in particular, the effect of AAC blending on $D_p/D_0(\varepsilon)$ relationships decreased. For most tested samples, pore-connectivity factor and diffusion-based tortuosity (T) gradually increased with drying, and T values were decreased slightly by blending with AAC grains. Equivalent pore diameter for gas flow values of graded RC and RCB showed a clear decrease with drying; on the other hand, those of AAC blended RC and RCB did not depend on ε. Combining previous models and fitted $T(\varepsilon)$ relations for tested samples, the $D_p/D_0(\varepsilon)$ relations and MLWs for $k_a(\varepsilon)$ captured well the values of graded RC and RCB blended with AAC grains, implying that the previous gas transport parameter models would be useful for quick assessment of roadbed materials.

Keywords: Gas transport parameters, Permeable pavement system, Construction and demolition waste, Autoclaved aerated concrete, Roadbed material, Pore tortuosity

1. INTRODUCTION

In order to reduce the surface temperature of paved surfaces and to mitigate the urban heat island effect, water-permeable and -retentive pavement systems have been investigated [1-4], and their applications to road construction are becoming popular [5-7]. The important mechanisms of the surface temperature reduction of road pavement systems are the surface gas exchange and vapor transport (i.e., evaporation) in the pavement systems, and the surface temperature reduction depends highly on the evaporation efficiency and water retention property of roadbed materials [8,9]. Many studies have been carried out to recycle construction and demolition waste (CDW) such as recycled concrete and clay bricks for road construction worldwide [e.g. 10-14] and to develop water-permeable and -retentive pavement systems utilizing various types of recycled materials from CDW, scrap construction materials [e.g., autoclaved aerated concrete (AAC)], and industrial by-products (e.g., steel slag) as roadbed materials [15-18]; however, most studies targeted mainly the hydraulic and mechanical properties of tested materials. Only limited information on gas transport parameters is available for roadbed materials in water-permeable and -retentive pavement systems, even though those parameters control the gas exchange and vapor transport processes and many researchers have proposed several gas transport parameters on soils or granular materials such as gas diffusivity (D_p/D_0: the ratio of gas diffusion coefficient, D_p, to gas diffusion in free air, D_0) and air permeability (k_a) [e.g. 19-25]. In this study, D_p/D_0, k_a, and their variations with air-filled porosity (ε) for graded recycled concrete (RC) and clay brick (RCB) aggregates, and RC and RCB blended with AAC grains at different proportions were examined in laboratory tests. In particular, the effect of including AAC grains on gas transport parameters and the ε dependency of gas transport parameters and pore structural parameters were examined based on previous $D_p/D_0(\varepsilon)$ and $k_a(\varepsilon)$ models.

2. MATERIALS AND METHODS

2.1 Materials

Waste concrete and clay bricks were taken from

CDW dumping sites in Hanoi, Vietnam (20° 59' 21.6" N, 105° 53' 58.1" E), and scrap autoclaved aerated concrete (AAC) collected from Viglacera Joint Stock Company in Bac Ninh Province, Vietnam (21°11'50.8"N, 106°00'42.8"E) were used in this study. All materials were crushed by a jaw and hammer mill crusher and sieved to adjust target particle size distributions for graded road base materials as described in TCVN 8859 (2011) [26]. The samples were prepared as graded recycled concrete (RC) and recycled clay brick (RCB) aggregates with the particle size ranging from 0 to 40 mm and AAC grains with the particle size ranging between from 0.106 to 2 mm. Photos of prepared samples are shown in Fig. 1, and the particle size distributions for graded RC, RCB, and AAC grains are shown in Fig. 2 together with the upper and lower boundaries of particle size distributions for road base materials described in TCVN 8859 (2011) [26].

Basic physical and chemical properties of RC, RCB, and AAC are summarized in Table 1. The pH values of RC and RCB were high due to cement and mortar adhering to the waste clay brick. On the other hand, the pH of AAC was lower than the others. The water absorption (w_{abs} in %) of AAC was much higher compared to RC and RCB. This is due to meso- and micropores rich in AAC grains and contributed to the water absorption [27]. In addition, w_{abs} of RCB was slightly higher than that of RC. This may be attributed to inherent micro-cracks inside the RCB aggregates.

Seven samples were used for a series of gas transport measurements in this study: a single material (RC 100%, RCB 100%, and AAC 100%) and AAC blended with RC and RCB at two different proportions, 20% and 40% (RC 80%+AAC 20%, RC 60%+AAC40%, RCB 80%+AAC 20%, and RCB 60%+AAC 40%). Here, the blending of AAC with high w_{abs} was expected to improve the water retention capacity of tested samples [15].

(a) RC aggregate (0-40 mm) (b) RCB aggregate (0-40 mm) (c) AAC grains (0.106-2 mm)

Fig.1. Tested materials: (a) graded recycled concrete (RC) aggregate, (b) graded recycled clay brick (RCB) aggregate, and (c) autoclaved aerated concrete (AAC) grains.

Table 1. Basic physical and chemical properties of recycled concrete (RC), recycled clay brick (RCB), and autoclaved aerated concrete (AAC) used in this study.

Samples	G_s	w_{AD} (%)	w_{abs} (%)		pH*	EC (mS/cm)	LA (%)
			< 4.75 mm	≥ 4.75 mm			
RC	2.63	0.8	8.5	5.2	11.2	4.8	38
RCB	2.64	0.3	14	13	10.7	0.0	46
AAC	2.51	2.1	61	-	9.0	0.9	56

G_s: specific gravity, w_{AD}: air-dried water content, w_{abs}: water absorption capacity, EC: electric conductivity, LA: Los Angeles abrasion. *pH in 1 mol KCl solution

2.2 Measurement of Gas Transport Parameters

For all tested samples, a compaction test (56 blows with a 4.5 kg rammer from a height of 450 mm of material in a cylindrical stainless mold with an inner diameter of 150 mm and height of 120 mm) [28, 29] was first carried out to determine compaction curves and the maximum dry bulk density (ρ_{dmax}) and optimum moisture content (OMC). The measured compaction curves are shown in Fig. 3. Except for RC 100%, the ρ_{dmax} and OMC of the tested samples were not clear. It is noted that the measured dry densities decreased

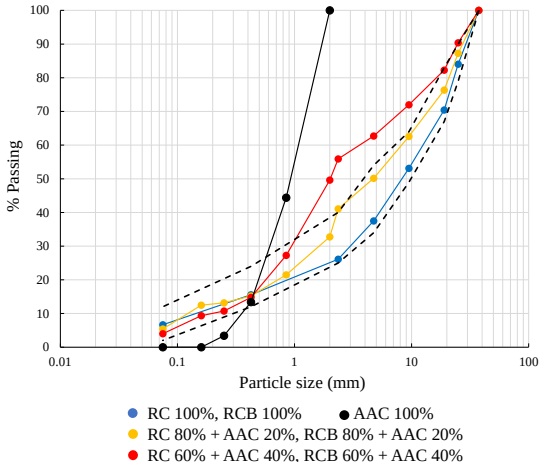

Fig.2. Particle size distributions of tested samples. Broken lines represent the upper and lower boundaries of particle size distribution for road base materials prescribed in TCVN 8859 (2011) [26].

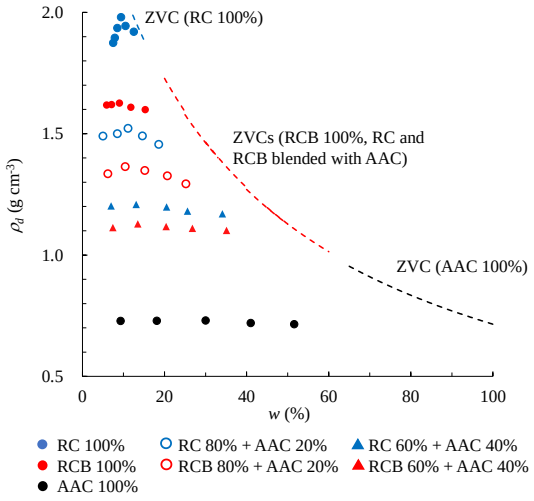

Fig.3. Compaction curves for tested samples. Zero void curves (ZVCs) for RC 100%, AAC 100%, and RC and RCB blended with AAC are shown by broken curves.

with increased proportions of AAC grains for both grades RC and RCB.

Then, the gas transport parameters during the drying of samples from saturation to air-dry compacted at the approximate OMC were measured. The compacted samples were soaked in water for one week to achieve saturation. The samples were dried using a combination of sandbox (0 and 6 kPa in suction), pressure chamber (10, 100, and 1000 kPa in suction), and air-drying (> 1000 kPa in suction). At the equilibrium of each suction level, the gas diffusion coefficient (D_p) and air permeability (k_a) were measured in a climate controlled room at 20°C and 60% relative humidity.

D_p was measured by a diffusion chamber method [30]. Oxygen gas was used in the assay, and D_p was calculated according to the method of Osozawa [31]. The k_a was measured by a constant air head method [32].

The air flow was supplied by an air compressor with constant pressure, and k_a was calculated by Darcy's law.

2.3 Gas Transport Parameter Models and Pore Structural Parameters

Power-law type models are commonly used to predict $D_p/D_0(\varepsilon)$ for porous materials including soils:

$$D_p/D_0 = \varepsilon^{X_g} \quad (1)$$

where X_g is an exponent corresponding to the pore connectivity-tortuosity factor for gas diffusivity. In general, the X_g values used were typically either 2 (Buckingham [19]) or 1.5 (Marshall [21]). Moldrup

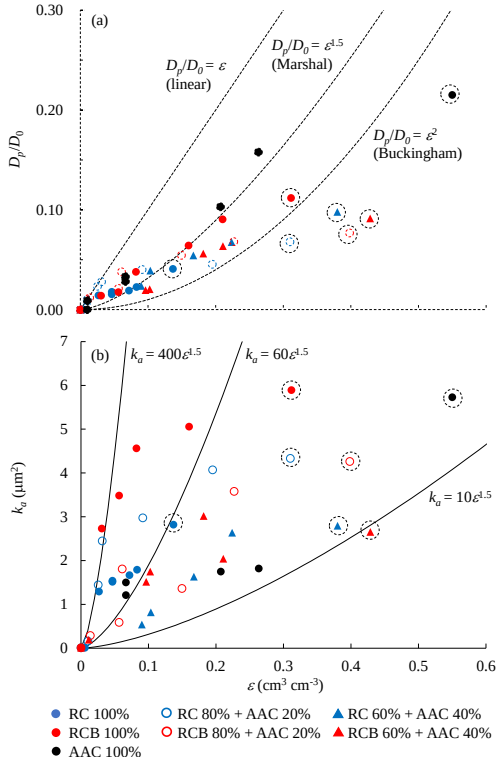

Fig.4. (a) Gas diffusivity (D_p/D_0) as a function of air-filled porosity (ε) for tested samples. The Marshal (1959) model [22], Buckingham (1904) model [21], and a linear line are given. (b) Air permeability (k_a) as a function of air-filled porosity (ε) for tested samples. Power-law curves ($k_a = \alpha\varepsilon^{Xa}$ [27-29]) with $X_a = 1.5$ and $\alpha = 10$, 60, and 400 are given. Note that measured values in air-dried condition are enclosed in dashed circles.

et al. [33] proposed a $D_p/D_0(\varepsilon)$ model using a diffusion-based tortuosity, T, assuming that pores of porous medium consist of tortuous and non-constricted tubes with uniform and similar diameters [34, 22]:

$$D_p/D_0 = \varepsilon T^{-2} \quad (2)$$

where T is the ratio of the average capillary tube length (L_e) to the length of the porous media (L), and can be calculated using measured D_p/D_0 data:

$$T = L_e/L = \left(\varepsilon D_0/D_p\right)^{0.5} \quad (3)$$

If T is expressed by an exponential function of $a\varepsilon^b$, the $D_p/D_0(\varepsilon)$ can be found by using Eq. (2):

$$D_p/D_0 = \varepsilon\left(a\varepsilon^b\right)^{-2} \quad (4)$$

Furthermore, Millington and Quirk [22] and Ball [35] suggested the equivalent pore diameter for gas flow, d_{eq}, based on Fick's law and Poiseuille's law and correlated the D_p/D_0 and k_a:

$$d_{eq} = 2\left[8\,k_a/\left(D_p/D_0\right)\right]^{0.5} \quad (5)$$

Combining Eqs. (4) and (5), a new $k_a(\varepsilon)$ model can be derived:

$$k_a = \left[\left(d_{eq}\right)^2 \varepsilon\left(a\varepsilon^b\right)^{-2}\right]/32 \quad (6)$$

3. RESULTS AND DISCUSSION

3.1 Measured Gas Diffusivity and Air Permeability and their Dependence on Air-filled Porosity

The measured D_p/D_0 values ranged mostly between a linear (i.e., $D_p/D_0 = \varepsilon$) and a Marshal model ($D_p/D_0 = \varepsilon^{1.5}$ [21]) at $\varepsilon < 0.1$ and ranged between a Marshal model and a Buckingham model ($D_p/D_0 = \varepsilon^2$ [19]) at $\varepsilon \geq 0.1$, except for the values measured in the air-dried condition (Fig. 4a). The D_p/D_0 values of RC blended with AAC grains did not show a clear difference in $D_p/D_0(\varepsilon)$ relationships. However, the values of RCB-blended AAC grains decreased slightly with increasing proportions of AAC grains.

A power law–type model, $k_a = \alpha\varepsilon^{Xa}$ [25, 36,37], was used to give the upper and lower boundaries of measured k_a values for tested samples (Fig. 4b). The X_a represents the pore connectivity-tortuosity for air convection, and X_a = 1.5 was chosen analogous to the Marshal model [21]. The measured k_a values ranged mostly from α = 10 to α = 400. Similar to the $D_p/D_0(\varepsilon)$ relations, the effect of blending with AAC grains on $k_a(\varepsilon)$ relationships was not observed for RC blended with AAC grains. For RCB, the measured k_a values were decreased by blending with AAC grains, but there was no significant difference in the measured values of RCB 80% + AAC 20% and RCB 60% + AAC 40%.

3.2 Pore Structural Parameters Based on Gas Transport Parameter Models

The ε dependence of gas transport parameters (D_p/D_0 and k_a) during the drying process and the blending of AAC grains with RC and RCB aggregates are controlled highly by changes of the pore network structure such as pore diameter, tortuosity, and connectivity. In this study, three pore

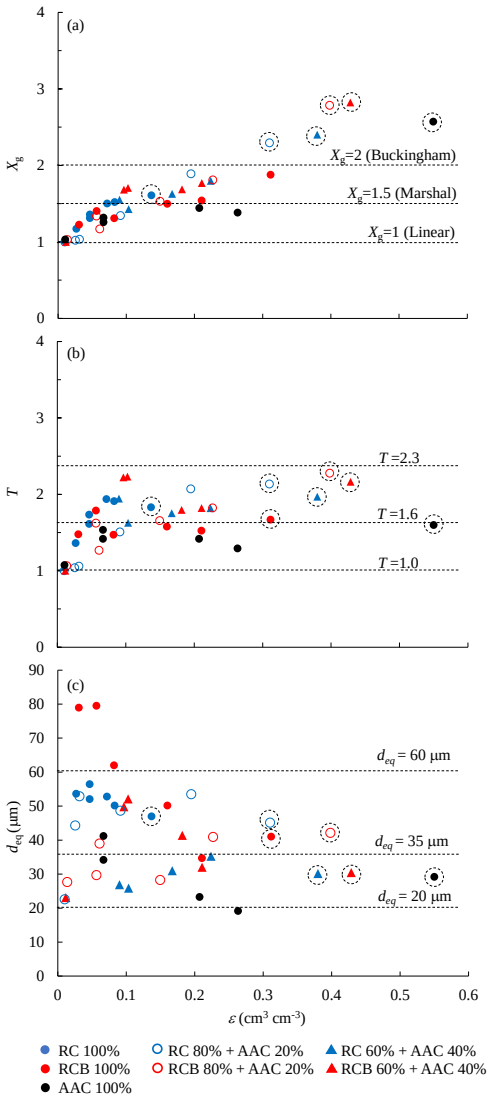

Fig.5. (a) Pore connectivity-tortuosity factor (X_g), (b) diffusion-based tortuosity (T), and (c) equivalent pore diameter for gas flow (d_{eq}) as a function of air-filled porosity (ε). Note that measured values in air-dried condition are enclosed in dashed circles.

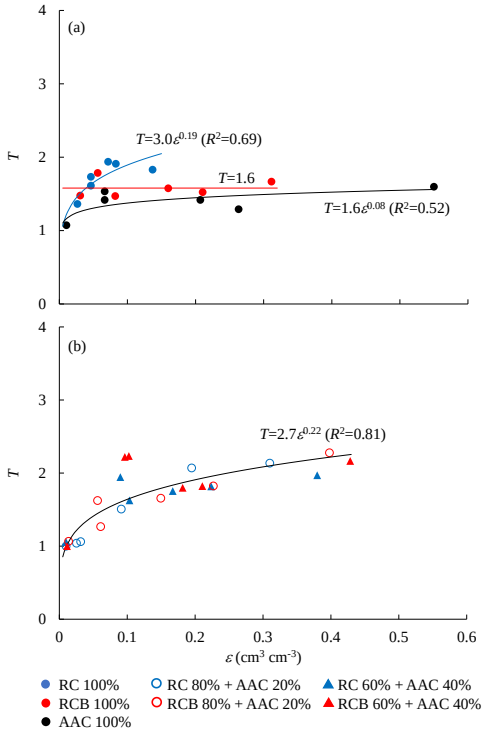

Fig.6. Fitted exponential curves to $T(\varepsilon)$ relationships: (a) RC 100%, RCB 100%, and AAC 100%, (b) RC and RCB samples blended with AAC grains. Note that T values for RCB 100% became almost constant (=1.6).

structural parameters, X_g [Eq. (1)], T [Eq. (3)], and d_{eq} [Eq. (5)], were examined based on the previous gas transport parameter models. The pore structural parameters calculated using measured D_p/D_0 and k_a values are shown in Fig. 5. The pore connectivity-tortuosity factor (X_g) increased gradually with increasing ε (i.e., drying) (Fig. 5a). The X_g values ranged mostly from 1 to 1.5 at $0 < \varepsilon < 0.10$ and ranged from 1.5 to 3.0 at $\varepsilon \geq 0.1$. In $X_g(\varepsilon)$ relationships, there was no significant effect of AAC blending with graded RC and RCB aggregates. Similar to $X_g(\varepsilon)$ relationships, diffusion-based tortuosity (T) increased with increasing ε and ranged mostly from 1.0 to 2.3, with an average value of 1.6 (Fig. 5b). It can be seen that the T values were decreased slightly by blending AAC grains with both RC and RCB aggregates. It is noted that the measured $T(\varepsilon)$ relations in this study were opposite to the reported data from soil samples [33], meaning that the pores of soil samples reportedly became less tortuous with drying, but the pores of our tested samples became more tortuous with drying. This might have enhanced the connection of micropores of RC and RCB aggregates and AAC grains during the drying process and have resulted in a more tortuous pore network in the drier condition. The values of equivalent pore diameters for gas flow (d_{eq}) of graded RC and RCB showed a clear decrease with drying and ranged from 45 to 60 μm for 100% RC and from 35 to 80 μm for 100% RCB. However, the RC and RCB aggregates blended with AAC grains did not show the ε dependence and ranged mostly from 20 to 60 μm (Fig. 5c). This suggests that the connected pores of AAC-blended samples became more uniform due to the water drainage from AAC grains during the drying process.

Categorizing the tested samples into three groups, RC 100%, AAC 100%, and RC and RCB samples blended with 20% and 40% AAC grains, an exponential function of $T = a\varepsilon^b$ was fitted to the calculated T and is shown in Fig. 6. The exponential function fitted the T values well and represented the ε dependence of T. It is noted that the T values were independent of ε for 100% RCB, and a simple constant value of 1.6 is given (Fig. 6a). In the exponential function, higher a and b increased e more with increasing ε. It can be seen clearly that the mixing proportion of AAC did not affect the $T(\varepsilon)$ and a single exponential equation, $T = 2.77\varepsilon^{0.22}$ ($R^2 = 0.81$), captured the $T(\varepsilon)$ relations of graded RC and RCB blended with AAC grains (Fig. 6b) well.

3.3 Estimation of Gas Transport Parameter Models

By combining the previous D_p/D_0 model and fitted $T(\varepsilon)$ relationships of tested samples in Fig. 6, the

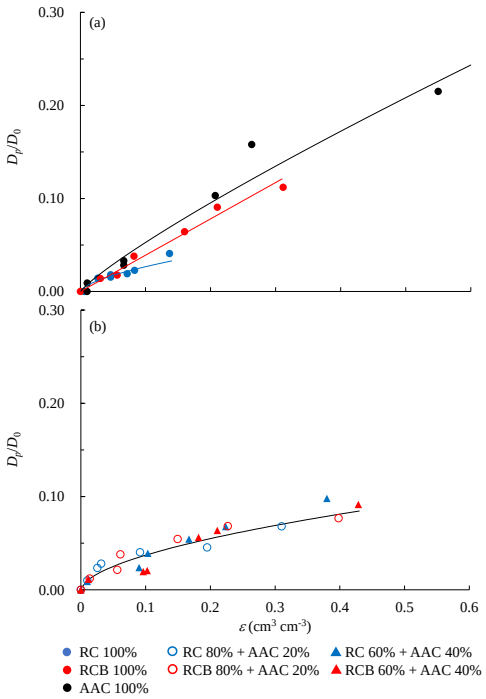

Fig.7. Fitting curves calculated from Eq. (4): (a) RC100%, RCB 100%, and AAC 100%, (b) RC and RCB samples blended with AAC grains.

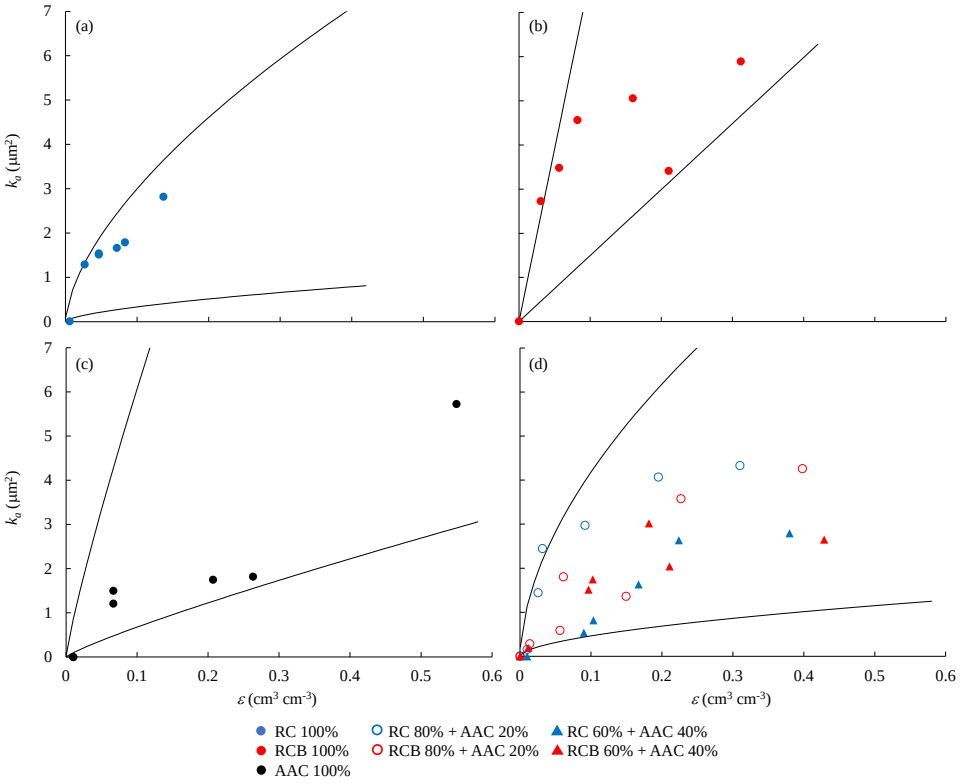

Fig.8. Most likely windows for measured k_a values: (a) RC 100%, (b) RCB 100%, (c) AAC 100%, and (d) RC and RCB blended with AAC grains.

fitness between measured $D_p/D_0(\varepsilon)$ data and Eq. (4) is illustrated in Fig. 7. Eq. (4) estimated the $D_p/D_0(\varepsilon)$ relationships well for all tested samples at a whole range of ε (i.e., from saturation to air-dry), suggesting that the accurate evaluation of $T(\varepsilon)$ relationships is important to predict the $D_p/D_0(\varepsilon)$ of graded aggregates and their AAC blended samples. Using the observed d_{eq} range of tested samples and fitted $T(\varepsilon)$ relationships shown in Fig. 6, the $k_a(\varepsilon)$ relations were calculated by Eq. (6) and the results shown in most likely windows (MLWs) for $k_a(\varepsilon)$ are illustrated in Fig. 8. The MLWs captured the upper and lower boundaries of k_a values at a whole range of ε values, suggesting that Eq. (6) would be a useful tool for quick assessment of the air permeability of graded RC and RCB as roadbed materials.

4. CONCLUSIONS

In this study, gas transport parameters for graded aggregates and their AAC-blended samples were measured during the drying process from saturation to air-dry in the laboratory, and the pore structural parameters were examined.

The results showed that the gas transport parameters of graded RC and RCB mostly decreased with increasing proportions of AAC grains, but the effect of AAC blending on gas diffusivities decreased. The pore structural parameters derived from previous gas transport parameter models characterized well the pore structure network of tested samples. Remarkably, the pores of our tested samples became more tortuous with drying in contrast to the results in [23], probably because the connection of micropores of RC and RCB aggregates and AAC grains during the drying process and have resulted in a more tortuous pore network in the drier condition. It was pointed out that accurate evaluation of diffusion-based tortuosity (T in Moldrup et al. 2001 [23]) is important to predict the gas diffusivity and to quickly assess the air permeability of graded aggregates and their AAC-blended samples as roadbed materials. Especially, the gas diffusivity and the air permeability of RC and RCB blended with AAC samples could be predicted uniformly regardless of the content of AAC grains. In order to have an accurate prediction of gas transport in roadbed materials and to apply the knowledge to evaluating the vapor and gas transport in the water permeable and retentive pavement systems, further studies are needed, especially for developing accurate predictive gas transport models that enable incorporation of vapor and gas, water, and heat transport processes in pavement systems.

5. ACKNOWLEDGMENTS

This research was supported by JST-JICA Science and Technology Research Partnership for Sustainable Development (SATREPS) project (No. JPMJSA1701).

6. REFERENCES

[1] Qin Y., He Y., Hiller J. E., and Mei G. A new water-retaining paver block for reducing runoff and cooling pavement. J. Clean. Prod., Vol. 199, Issue 20, 2018, pp. 948-956.

[2] Santamouris M. Using cool pavements as a mitigation strategy to fight urban heat island - A review of the actual developments. Renew. Sustain. Energy Rev., Vol. 26, 2013, pp. 224-240.

[3] Yamagata H., Nasu M., Yoshizawa M., Miyamoto A., and Minamiyama M. Heat island mitigation using water retentive pavement sprinkled with reclaimed wastewater. Water Sci. Technol., Vol. 57, No. 5, 2008, pp. 763-771.

[4] Kim R., Park J. B., Mun J., and Lee. J. Reduction effects of urban heat island by water-retentive pavement. Mater. Sci. Forum, Vol. 724, 2012, pp. 147-150.

[5] Takahashi K., and Yabuta K. Road temperature mitigation effect of 'road cool,' a water-retentive material using blast furnace slag. JFE Tech. Rep., Vol. 13, 2009, pp. 58-62.

[6] Lin C. F., Wu C. H., and Ho H. M. Recovery of municipal waste incineration bottom ash and water treatment sludge to water permeable pavement materials. Waste Manag., Vol. 26, No. 9, 2006, pp. 970-978.

[7] Park J. B., Lee S., Gee C. S., and Pyun H. B. Experimental study of non-sintering block for reducing surface temperature using recycling bottom ash. Mater. Sci. Forum, Vol. 620-622, 2009, pp. 105-108.

[8] Kinoshita S., Yoshida A., and Okuno N. Evaporation performance analysis for water-retentive material, based on outdoor heat-budget and transport properties. J. Heat Isl. Inst. Int., Vol. 7, No. 2, 2012, pp. 222-230.

[9] Misaka I., Narita K., and Yokoyama H. Evaluation of evaporation ability of the system for mitigating urban heat island. 7th Int. Conf. Urban Clim., 2009, pp. 2-5.

[10] Kang D., Gupta S. C., Ranaivoson A. Z., Siekmeier J., and Roberson R. Recycled materials as substitutes for virgin aggregates in road construction: I. Hydraulic and mechanical characteristics. Soil Sci. Soc. Am. J., Vol. 75, No. 4, 2011, pp. 1265-1275.

[11] Rahardjo H., Vilayvong K., and Leong E. C. Water characteristic curves of recycled materials. Geotech. Test. J., Vol. 34, No. 1, 2011, pp. 89-96.

[12] Arulrajah A., Piratheepan J., Bo M. W., and Sivakugan N. Geotechnical characteristics of recycled crushed brick for pavement sub-base applications. Can. Geotech. J., Vol. 49, 2012, pp. 796-811.

[13] Tatsuoka F., Tomita Y., Iguchi Y., and Hirakawa D. Strength and stiffness of compacted crushed concrete aggregate. Soils Found. Vol. 53, No. 6, 2013, pp. 835-852.

[14] Mehrjardi G. T., Azizi A., Haji-Azizi A., Asdollafardi G. Evaluating and improving the construction and demolition waste technical properties to use in road construction. Transp. Geotech. Vol. 23, 2020, 100349.

[15] Kato A., Ito R., Matsuno A., Uchimura T., Nguyen V. T., Nguyen H.G., and Kawamoto K. Water retention and gas transport characteristics of recycled graded roadbed materials blended with AAC grains. Proceedings of 17th International Waste Management and Landfill Symposium (Sardinia 2019), 2019, 218.

[16] Rahman M.A., Imteaz M.A., Arulrajah A., Piratheepan J., and Disfani M.M. Recycled construction and demolition materials in permeable pavement systems: geotechnical and hydraulic characteristics. J. Clean. Produc. Vol. 90, 2015, pp. 183-194.

[17] Moriishi K., Ohnishi Y., Nishiyama S., Yano T., and Koseki H. Influence of type of granular materials on permeability and durability of permeable pavements. J. Pavement Eng, JSCE. Vol. 14, 2009, pp. 25-32 (In Japanese).

[18] Kuno A. and Tatebe H. Experimental study on the subbase and subgrade of permeable paving that utilized water granulated slag. Bulletin of Aichi Institute of Technology, Part B. Vol. 35, pp. 151-158 (In Japanese).

[19] Buckingham E. Contributions to our knowledge of the aeration of soils. U.S. Government Printing Office, 1904.

[20] Penman H. L. Gas and vapour movements in the soil: I. The diffusion of vapours through porous solids. J. Agric. Sci. Vol. 30, No. 3, 1940, pp. 437-462.

[21] Marshal T. J. The diffusion of gases through porous media. J. Soil Sci. Vol. 10, Issue 1, 1959, pp. 79-82.

[22] Millington, R.J. and Quirk J.M. Formation factor and permeability equations. Nature Vol. 202, 1964, pp. 143-145.

[23] Moldrup P., Olesen T., Gamst J., Schjonning P., Yamaguchi T., and Rolston D. E. Predicting the gas diffusion coefficient in repacked soil: Water-induced linear reduction model. Soili Sci. Soc. Am. J. Vol. 64, No. 5, 2000, pp. 1588-1594.

[24] Kawamoto K., Moldrup P., Schjonning P., Iversen B. V., Komatsu T., and Rolston D. E. Gas transport parameters in the vadose zone:

Development and tests of power-law models for air permeability. Vadose Zone J. Vol. 5, No. 4, 2006, pp. 1205-1215.

[25] Hamamoto S., Moldrup P., Kawamoto K., Schjonning P., and Komatsu T. Two-region extended Archie's law model for soil air permeability and gas diffusivity. Soil Sci. Soc. Am. J. Vol. 75, No. 3, 2011, pp. 795-806.[26] TCVN 8859-2011. Graded aggregate bases and subbases pavement - Specification for construction and acceptance. 2011 (in Vietnamese).

[27] Nguyen T. L., Asamoto S., and Masui K. Microstructure and shrinkage behavior of autoclaved aerated concrete (AAC) – Comparison of Vietnamese and Japanese AACs–, J. Adv. Concr. Technol., Vol. 16, 2018, pp. 333-342.

[28] ASTM, D1557-12. Standard test methods for laboratory compaction characteristics of soil using modified effort. ASTM International, West Conshohocken, PA, 2012.

[29] 22TCN 333-06. The standard method used related compaction of the material in a series of layers in a fixed mould. 2006 (in Vietnamese).

[30] Rolston, D.E., and Moldrup P. Gas diffusivity. In J.H. Dane and G.C. Topp (ed.) Methods of Soil Analysis, Part 4, SSSA Book Ser.5. SSSA, Madison, WI, pp. 1113-1139.

[31] Osozawa, S. Measurement of soil-gas diffusion coefficient for soil diagnosis, (In Japanese with English summary.) Soil Phys. Cond. Plant Growth. Vol. 55, 1987, pp. 53-60.

[32] Iversen B.V., Schjonning P., Poulsen T.G. and Moldrup P. In Situ, on-site and laboratory measurements of soil air permeability: Boundary conditions and measurement scale. Soil Sci. Vol. 166, No. 2, 2001, pp. 97-106.

[33] Moldrup P., Olesen T., Komatsu T., Schjonning P., and Rolston D. E. Tortuosity, diffusivity, and permeability in the soil liquid and gaseous phases. Soil Sci. Soc. Am. J. Vol. 65, Issue 3, 2001, pp. 613-623.

[34] Currie, J. A. Gaseous diffusion in porous media. Part 2. - Dry granular materials. Brit. J. Appl. Phys. Vol. 11, No. 8, 1960, pp. 318-325.

[35] Ball B. C. Modelling of soil pores as tubes using gas permeabilities, gas diffusivities and water release. Euro. J. Soil Sci. Vol. 32, No. 4, 1981, pp. 465-481.

[36] Wickramarachchi, P., Kawamoto K., Hamamoto S., Nagamori M., Moldrup P., and Komatsu T. Effects of dry bulk density and particle size fraction on gas transport parameters in variably saturated landfill cover soil. Waste Manag. Vol. 31, 2011, pp. 2462-2472.

[37] Baniya A., Kawamoto K., Hamamoto S., Sasaki T., Saito T., Muller K., Moldrup P., and Komatsu T. Linking pore network structure derived by microfocus X-ray CT to mass transport parameters in differently compacted loamy soils. Soil Res. Vol. 57, 2019, pp. 642-656.